Geophysical Journal International

Geophys. J. Int. (2015) **200,** 1003–1009 doi: 10.1093/gji/ggu440

GJI Geomagnetism, rock magnetism and palaeomagnetism

Accelerating EM integral equation forward solver for global geomagnetic induction using SVD based matrix compression method

Jin Sun and Alexey Kuvshinov

ETH Zurich, Institute of Geophysics, Sonneggstrasse 5, 8092 *Zurich, Switzerland. E-mail: sunjin09@gmail.com*

Accepted 2014 November 11. Received 2014 November 7; in original form 2014 February 12

SUMMARY

We develop an singular value decomposition-based compression of the Green's function matrix of an electromagnetic integral equation forward solver for global geomagnetic induction, on top of an fast Fourier transform reduction of the system to a block-diagonal form. With this approach, the memory usage and CPU time of Krylov subspace iterative solutions are significantly reduced at a very small cost of accuracy, making the accelerated forward solver well suited for 3-D inversions as well as forward simulations with multiple sources.

Key words: Numerical solutions; Electromagnetic theory; Geomagnetic induction.

1 INTRODUCTION

Frequency-domain integral equation (IE) based electromagnetic (EM) forward solvers, known for their high accuracy and numerical stability, flexible discretization, as well as compact computational domain with exact boundary conditions for open domain problems, find their applications in geo-EM induction at both local and global scales (Fainberg *et al.* 1990; Pankratov *et al.* 1995; Singer 1995; Koyama 2001; Avdeev *et al.* 2002; Hursan & Zhdanov 2002; Kuvshinov *et al.* 2002; Kuvshinov 2008; Singer 2008; Sun & Egbert 2012a; Koyama *et al.* 2014, among others).

However, a known drawback of such methods is the large computational complexity, since EM Green's functions, central to the IE formulation, are global operators that, after discretization, result in full system matrices. Fortunately, certain properties of typical EM Green's functions allow efficient storage and fast application (multiplication of some vector) of such operators, leading to fast implementation of iterative solutions, for example Krylov subspace methods, to the IE. One such property is the shift invariances of the Green's functions defined on regular grids under invariant background geometries, for example shift invariances in lateral dimensions for horizontally layered structures under cartesian geometry, and rotational invariance under spherically layered geometry. Such invariances allow applications of the Green's functions to be implemented as linear or circular convolutions using fast Fourier transform (FFT). However, when such invariances are not available either due to shift-variant grids or shift-variant background geometries, FFT cannot be directly applied. In such more general cases, another property, the diagonal dominance of the Green's functions, is often employed. The diagonal dominance is the result of a general phenomenon that EM field responses of a collection of sources reduce with distance. This is especially true for quasi-static interactions in lossy media, as is the case in geomagnetic induction. When the sources are sufficiently separated from the observations, the observed EM field has a much smaller degree of freedom than the total number of possible configurations of the sources. The field can thus be computed from a reduced number of equivalent sources with reduced computational complexity and memory requirement.

Acceleration methods based on such considerations are numerous, see Chew *et al.* (1997) for a review. Two such methods widely used in high-frequency EM forward modelling (e.g. optical and microwave scattering) include: fast multipole algorithm (FMA) and varieties (Rokhlin 1990; Lu & Chew 1994, among others), which develop analytic local and multipole expansions of Green's functions of known analytic forms; and matrix decomposition algorithm (MDA) and varieties (Michielssen & Boag 1994, 1996; Rius *et al.* 2008, among others), which develop expansions of the Green's functions using numerical linear algebra techniques. While the multilevel variety of FMA is asymptotically slightly faster than the multilevel MDA for very large scale EM scattering problems, the matrix decomposition methods are more straightforward to apply to existing implementations of IE solvers, and should work very effectively for quasi-static EM induction problems involving lossy media.

In this work, we apply a singular value decomposition (SVD) based matrix compression method to an IE forward solver for global geomagnetic induction: After employing rotational invariance of the Green's function of a spherical Earth by applying FFT in the longitudinal direction, the reduced system is further compressed using a divide-and-conquer approach based on SVD low-rank approximations with controlled errors in terms of Frobenius norm, leading to a recursively compressed form of the Green's function matrix that is computationally efficient.

The remainder of this paper is organized as follows. In Section 2, we summarize theory of an iterative forward solver of IE-based global geomagnetic induction based on an affine-transformed Green's function as a contracting operator. In Section 3, we develop recursive compression of the contracting operator, and apply to the solution of the IE using Krylov subspace method, within the context of a simplified scalar model for illustration. In Section 4, we illustrate with numerical examples on the scalar case, and in Section we report progresses towards implementations in the realistic case.

2 THEORY OF THE FORWARD MODEL

In this section, we present the forward model in the frequency domain, with harmonic time dependence $e^{-i\omega t}$. Maxwell's equations in a non-magnetic linear conductive medium may be expressed as

$$\nabla \times \mathbf{H} = \mathbf{J}_s + \sigma \mathbf{E}, \tag{1}$$

$$\nabla \times \mathbf{E} = i\omega\mu_0 \mathbf{H}, \tag{2}$$

where μ_0 is the permeability of the free space, σ is the inhomogeneous conductivity of the medium, and $\mathbf{E}$, $\mathbf{H}$ and $\mathbf{J}_s$ are the complex electrical field, magnetic field and exciting current source. Note that in geomagnetic induction, the displacement current within a conductive medium is ignored. Substituting (2) into (1) leads to the vector wave equation for $\mathbf{E}$

$$\nabla \times \nabla \times \mathbf{E} - k_b^2 \mathbf{E} = i\omega\mu_0(\mathbf{J}_s + \Delta\sigma \mathbf{E}), \tag{3}$$

where $\sigma = \sigma_b + \Delta\sigma$ has been separated into the sum of a background and a perturbative part, and $k_b = \sqrt{i\omega\mu_0\sigma_b}$ is the background complex wave number. Solution to (3) is best described in terms of the electric tensor Green's function, which satisfies

$$\nabla \times \nabla \times \mathbb{G}(\mathbf{r}, \mathbf{r}') - k_b^2 \mathbb{G}(\mathbf{r}, \mathbf{r}') = i\omega\mu_0 \mathbb{I}(\mathbf{r}, \mathbf{r}'), \tag{4}$$

where $\mathbb{I}(\mathbf{r}, \mathbf{r}') := \mathbf{I}\delta(\mathbf{r}, \mathbf{r}')$ is the kernel of the identity operator, with $\mathbf{I}$ being the 3×3 identity matrix and $\delta(\mathbf{r}, \mathbf{r}')$ the 3-D Dirac delta function. Explicit form of $\mathbb{G}(\mathbf{r}, \mathbf{r}')$ may be found in, for example, Sun & Egbert (2012b) and Kuvshinov & Semenov (2011). Following standard procedures, one obtains from (3) and (4) the IE satisfied by $\mathbf{E}$,

$$\mathbf{E} = \mathbf{E}_b + \mathbb{G}(\Delta\sigma \mathbf{E}), \tag{5}$$

where $\mathbb{G}(\mathbf{J}) := \int d^3r' \mathbb{G}(\mathbf{r}, \mathbf{r}') \cdot \mathbf{J}(\mathbf{r}')$, where $\mathbf{J}$ represent the primary or secondary electric current field, and $\mathbf{E}_b := \mathbb{G}(\mathbf{J}_s)$ is identified as the primary (background) electric field generated by the source current $\mathbf{J}_s$ with the absence of conductivity perturbation, that is $\Delta\sigma = 0$. The forward problem of geomagnetic induction consists of solving (5) for the electric field $\mathbf{E}$ (and subsequently for $\mathbf{H}$ through (1)), given knowledge of the conductivity perturbation $\Delta\sigma$ and the primary field $\mathbf{E}_b$.

A solution to the forward problem (5) may be obtained by applying a fixed point iteration on an appropriately transformed IE (Pankratov *et al.* 1995; Singer 1995, among others). Following notations in Sun & Egbert (2012b), this solution is given in terms of the renormalized field as

$$\mathbf{E}' = \sum_{n=0}^{\infty} (\upsilon\Gamma)^n (\mathbf{E}'_b), \tag{6}$$

where $\mathbf{E}'(\mathbf{r}) := \frac{\Delta\sigma}{\sigma_b}\mathbf{E}(\mathbf{r})$, $\mathbf{E}'_b(\mathbf{r}) := 2\upsilon\mathbf{E}_b(\mathbf{r})$ are the renormalized fields, $\upsilon := \frac{\Delta\sigma}{2\sigma_b + \Delta\sigma}$ is a multiplicative factor that satisfies $|\upsilon(\mathbf{r})| < 1$. The operator $\Gamma = 2\sigma_b\mathbb{G} + \mathbb{I}$, where $\mathbb{I}$ is the identity operator, has an L_2 operator norm $\|\Gamma\| \leq 1$. Consequently, $\upsilon\Gamma$ is a contraction operator, and (6) is convergent in L_2. The original electric field may be obtained as $\mathbf{E} = \frac{\sigma_b}{2\sigma_b + \Delta\sigma}[2\mathbf{E}_b + \Gamma(\mathbf{E}')]$, which is easily verified.

3 RECURSIVE SVD COMPRESSION OF THE ITERATIVE OPERATOR

In order to simplify our illustration of the recursive SVD compression scheme, we consider a scalar variant of the vector wave equation (3),

$$\nabla^2\Phi + k_b^2\Phi = -i\omega\mu_0(S_0 + \Delta\sigma\Phi), \tag{7}$$

where S_0 is some scalar source, and Φ the corresponding scalar field generated by this source. Following similar procedures as in the vector case by defining $\Phi' := \frac{\Delta\sigma}{\sigma_b}\Phi$, $\Phi'_b := 2\upsilon\Phi_b$ and making use of the scalar Green's function defined by

$$\nabla^2 g(\mathbf{r}, \mathbf{r}') + k_b^2 g(\mathbf{r}, \mathbf{r}') = -i\omega\mu_0\delta(\mathbf{r}, \mathbf{r}'), \tag{8}$$

an iterative solution to (7) may be obtained as

$$\Phi' = \sum_{n=0}^{\infty} (\upsilon\gamma)^n \Phi'_b, \tag{9}$$

with convergence guaranteed if the integral operator $\gamma = 2\sigma_b g + \delta$, where δ is the identity operator (Dirac delta), satisfies $\|\gamma\| \leq 1$, as is shown in Appendix A. We will use (9) in the following discussion, bearing in mind that implementation of (6) component-wise is completely analogous.

In an iterative computation of (9), at the jth iteration, the following operation,

$$\Phi'_j(\mathbf{r}) = \upsilon(\mathbf{r}) \int d^3r' \gamma(\mathbf{r}, \mathbf{r}')\Phi'_{j-1}(\mathbf{r}'), \tag{10}$$

must be evaluated. This is usually accomplished by discretizing on a 3-D uniform numerical grid of $L \times M \times N$ cells in r, θ, ϕ, respectively, leading to

$$\Psi'_j(r_l, \theta_m, \phi_n) = \sum_{l',m',n'=0}^{L,M,N} \gamma(r_l, \theta_m, \phi_n, r_{l'}, \theta_{m'}, \phi_{n'}) \times \Phi'_{j-1}(r_{l'}, \theta_{m'}, \phi_{n'}), \tag{11}$$

where $\mathbf{r} = (r, \theta, \phi)$ is discretized as (r_i, θ_j, ϕ_p) and $\mathbf{r}' = (r', \theta', \phi')$ as (r_k, θ_l, ϕ_q), and

$$\Phi'_j(r_l, \theta_m, \phi_n) = \upsilon(r_l, \theta_m, \phi_n)\Psi'_j(r_l, \theta_m, \phi_n) \tag{12}$$

is a point-wise multiplication. One of the simplest discretization schemes, which is adopted here, assumes that the field is constant over each cell, and takes average value of the kernel of the integral operator over each pair of source-field cells. Evidently evaluation of (11) is the most time-consuming part of implementing solution (6). To accelerate the matrix-vector multiplication (11), we observe the rotational invariance of a spherical layered Earth. This implies that the Green's function g as well as γ is shift invariant in ϕ, that is $\gamma(r_l, \theta_m, \phi_n, r_{l'}, \theta_{m'}, \phi_{n'}) = \gamma(r_l, \theta_m, r_{l'}, \theta_{m'}, \phi_n - \phi_{n'})$. Therefore, applying FFT with respect to ϕ to (11) leads to

$$\tilde{\Psi}'_j(r_l, \theta_m, n) = \sum_{l',m'=0}^{L,M} \tilde{\gamma}(r_l, \theta_m, r_{l'}, \theta_{m'}, n)\tilde{\Phi}'_{j-1}(r_{l'}, \theta_{m'}, n), \tag{13}$$

where the tilde'd quantities are FFT's of the original quantities, indexed by the discrete (spatial) frequency $2\pi n/N$, $n \in \{0, 1, \ldots, N-1\}$.

The block-diagonalized operator $\tilde{\gamma}$ may be compressed to further improve efficiency by observing its diagonal dominance, which is a consequence of reduced degrees of freedom when source and field domains are well separated. Intuitively, if a source domain Ω_s is well separated from a field (response) domain Ω_f, any source distribution in Ω_s may be represented, to a high degree of accuracy, as a linear combination of a reduced number of orthogonal basis sources, each of which has its independent response in Ω_f, and the total response is the linear combination of the independent responses. This reduces the computation of response in Ω_f from an arbitrary source in Ω_s into decomposing the source in terms of basis sources, accounting for responses from these basis sources and synthesizing these responses

to form the total response. Since both the basis sources and their responses may be computed *a priori*, the computational cost is reduced from a full operator-vector multiplication to a few dot products. In terms of (13), this is equivalent to approximating some off-diagonal subblock of the matrix $\tilde{\gamma}$, which is a full block, as a sum of rank-one matrices. Each rank-one matrix corresponds to one independent basis source. In practice, this is easily accomplished numerically through a truncated SVD of the corresponding matrix block.

To best utilize the reduced degrees of freedom for well separated source and field domains, a systematic domain decomposition, such as the binary decomposition scheme shown in Fig. 1, is developed. At each step, the current domain is divided into two disjoint subdomains, and their mutual interaction is accounted for using the corresponding matrix subblock of $\tilde{\gamma}$, which is simply the rank-deficient off-diagonal subblock shown in Fig. 2, with SVD compression. This procedure repeats on each subdomain at the next step. The simple scheme shown in Fig. 1 is by no means unique or optimal, and the flexibility of being able to accommodate arbitrary domain decomposition schemes is an advantage of the recursive SVD matrix compression method.

In this recursive compression procedure, the truncation errors are easily quantified by the sum of squares of the truncated singular values, leading to a quantification of errors in terms of squares of the Frobenius norms summable over subblocks. Specifically, if the maximal allowed error in terms of Frobenius norm of the matrix $\tilde{\gamma}$ is ϵ, each of the four subblocks as shown in Fig. 2 is allowed to have an error of $\epsilon/2$, and the total error is thus $\sqrt{4(\epsilon/2)^2} = \epsilon$. The off-diagonal subblocks are approximated by truncating their SVD at levels corresponding to a truncation error of $\epsilon/2$. The procedure is then applied to the diagonal subblocks with a total error of $\epsilon/2$ for each diagonal subblock. As the procedure is recursively applied until the diagonal subblocks become too small or the off-diagonal subblocks become rank sufficient, the total error of the original matrix is maintained at ϵ. This procedure leads to a compression of the original matrix $\tilde{\gamma}$ in terms of both storage and computational complexity of matrix–vector multiplication, with a prescribed error in Frobenius norm. Note that a more appropriate measure of compressional error may be given in terms of the L2 operator norm. In practice, compressional error in terms of Frobenius norm often serves as a conservative indication of L2 error in the solution caused by the compression, as is seen in the numerical examples presented in Section 4.

In theory, reduction ratios for memory usage and CPU time are the same, since for each matrix–vector multiplication, each element in the compressed Green's function matrix is multiplied exactly once. In practice, however, overhead involved in the recursive multiplication of the compressed matrix usually result in less-than-ideal CPU time improvements.

4 NUMERICAL IMPLEMENTATION IN THE 3-D SCALAR MODEL

To illustrate the procedures described in the preceding section, we consider a simple induction model of a two-layer spherical Earth, shown in Fig. 3, overlain by an inhomogeneous surface conductance shell, shown in Fig. 4. The interface between the core and the outer

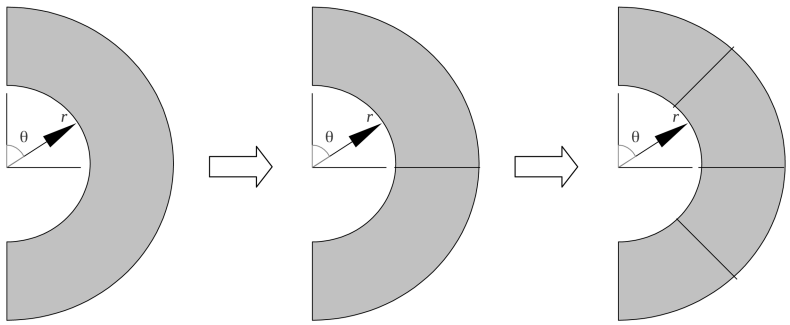

Figure 1. Illustration of a recursive binary decomposition of the (r, θ) domain.

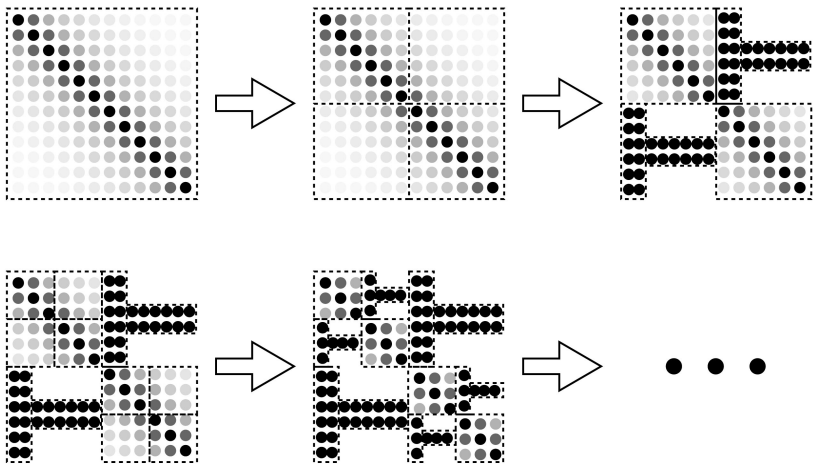

Figure 2. Illustration of a recursive binary decomposition of the $\tilde{\gamma}$ matrix.

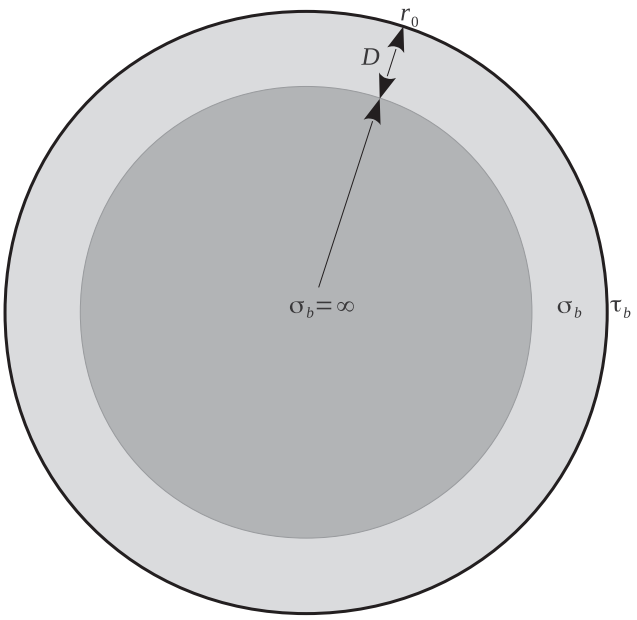

Figure 3. The two-layer background conductivity model.

layer is located at the depth $D = 850$ km. The core is assumed to be infinitely conductive, and the outer layer has a homogeneous background conductivity. Inhomogeneous conductivity perturbations are restricted to the outer layer. For simplicity, we chose a fixed background conductivity $\sigma_b = 0.15\ \mathrm{S\,m^{-1}}$ for all the perturbations we tested with. The choice of surface background conductance is $\tau_b = 8000$ S. The model is discretized on a regular spherical grid of $N_\theta \times N_\phi \times N_r$, where $N_\theta = 128$, $N_\phi = 256$ and $N_r = 16$.

In the forward simulations, a standard dipole source Y_1^0 at 6-d period was assumed. A conductivity anomaly slap (Fig. 4) of 6 km in thickness with a conductivity contrast of 10 × was introduced at different depths ranging from 24.8 to 817.3 km. Forward simulated surface data of scalar field Φ were shown in Fig. 5, where deeper anomalies have less effects observed from the surface, as a result of reduced interactions with distance. Simulation time and accuracy were summarized in Table 1.

Two observations can be made from this comparison. First, relative L2 errors in the forward-simulated surface data caused by the compression of Green's function matrix are much smaller than the compression error of the Green's function matrix. Possible reasons include: (i) compressional errors in terms of Frobenius norm may be a conservative estimate of errors of forward solutions in terms of L2 norm, as is noted in the preceding section and (ii) surface data are relatively insensitive to anomalies at depths, due to reduced interaction at distance, implying that errors of forward solutions caused by inaccurately represented interactions at depths do not effectively propagate to the surface. Secondly, even though errors of forward solutions seem to increase with increasing levels of compression, the corresponding CPU time is not monotonically decreasing as one would expect, leading to a 'saturation' of compression at least in terms of CPU time reduction. This is due to implementation-dependent computational overhead involved in the matrix–vector multiplication of the compressed matrix, such as indexing, caching, etc.

5 TOWARDS IMPLEMENTATION IN A REALISTIC 3-D VECTOR MODEL

The recursive compression scheme described in the previous sections may be extended to a realistic vector EM induction model. The 3-D tensor Green's function of such a model consists of six independent components, if symmetry has been taken into considerations. Each component may be viewed as a stand-alone scalar operator that may be discretized, leading to a diagonal dominant matrix with symmetric structures, which may be independently compressed, similar to the case of the scalar model. To test the compression, we have computed the tensor Green's function matrix of a full EM induction realistic forward model based on a 3-D vector IE Kuvshinov (2008). The tensor Green's function was computed with the same conductivity model at the same period and discretized on the same numerical grid as in the scalar case. We have tested the compression on the $\phi\phi$ component of the tensor Green's function. The compression errors and corresponding compression ratios are given by Table 2, where we also included CPU time measurements as well as L2 errors of the matrix-vector multiplication on a random vector. Full implementation of the forward iterative solver will be presented in a future work.

In the compression of the tensor Green's function, we have adopted a different error allowance scheme. Recall that in implementing (13) the compression was applied to each Fourier component $\tilde{\gamma}(n)$. In the scalar case, these Fourier components share the same *relative* compression error, while in the tensor case, they share the same *absolute* compression error, with the overall error kept at the same relative level. This implies lower relative error at low frequency components, due to a fast decay of energy towards high-frequency components. Compression ratio can be significantly enhanced at relatively higher error levels, as is evident from Table 2 compared with Table 1. It is also noted that the relative L2 error listed in the two tables are different measures: In Table 1, L2 errors were measured in the forward solution at the surface of the Earth, while in Table 2, they are measured in the entire domain. Due to insensitivity of the surface field to deeper interactions, Table 1 exhibits significantly lower L2 errors. These observations imply

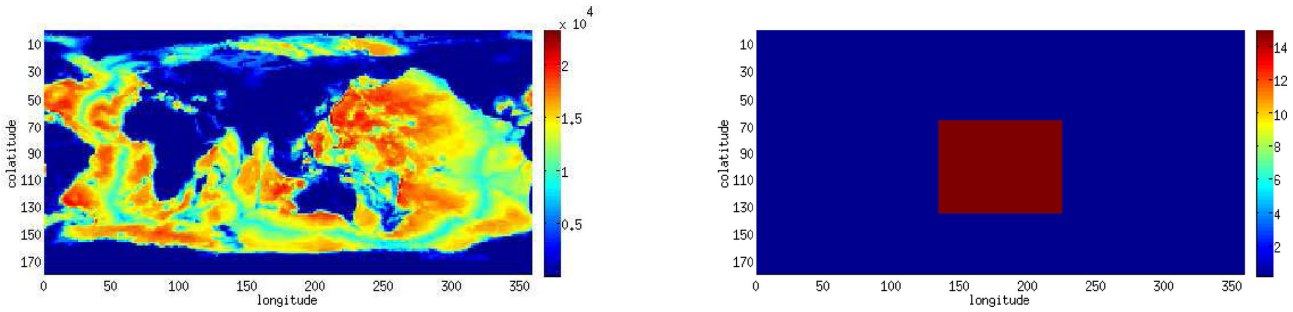

Figure 4. The surface conductance map (left-hand panel) and the horizontal map of the anomaly (right-hand panel).

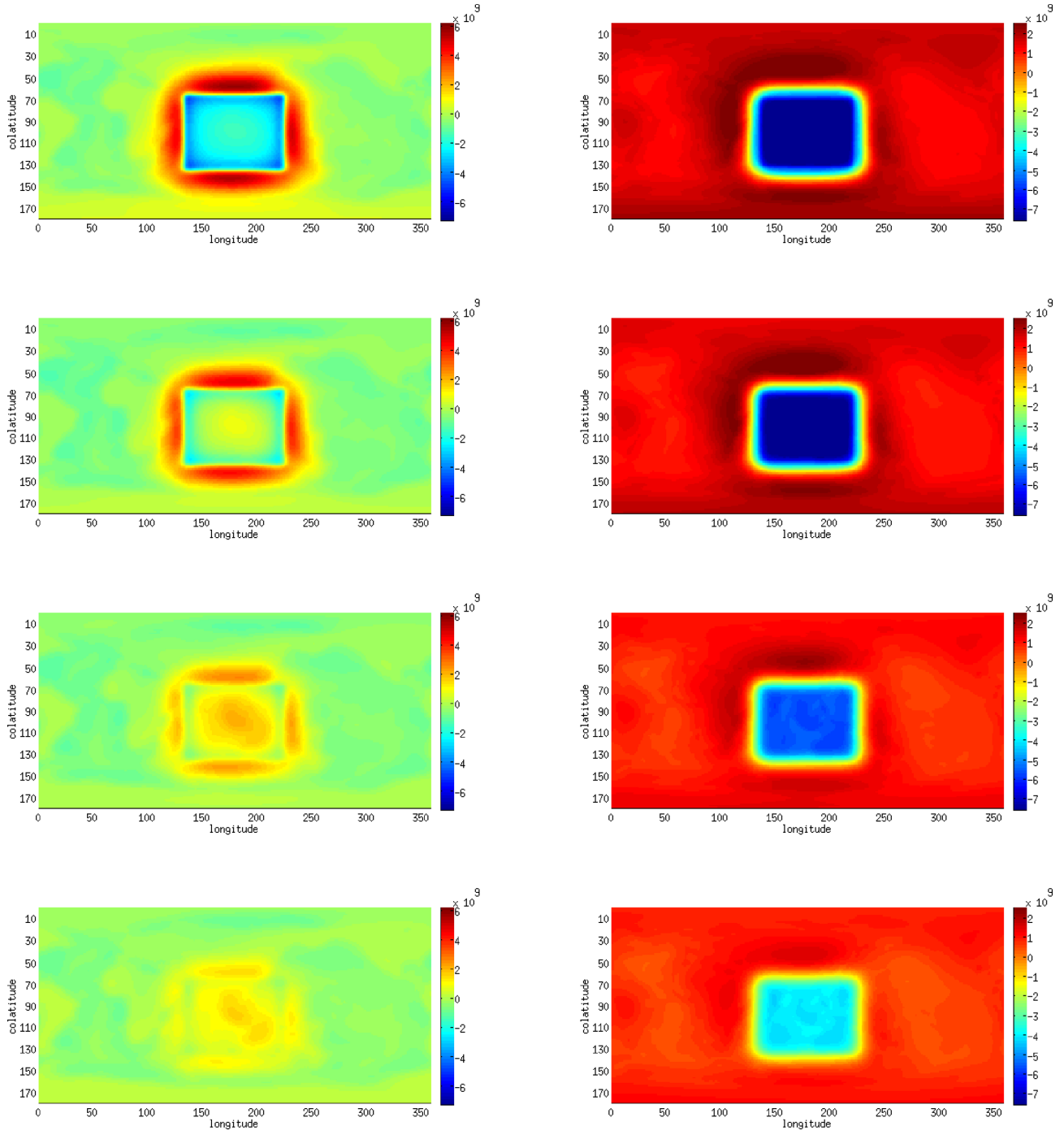

Figure 5. The forward-simulated scalar field Φ at the surface: From top to bottom, anomaly is located at 126, 231, 452 and 690 km depths. Left- and right-hand panels correspond to real and imaginary parts.

Table 1. Comparison of forward solutions among different levels of compression for the scalar Green's function discretized on the 128 × 256 × 16 numerical grid.

Compression error	0 per cent	0.1 per cent	1 per cent	5 per cent
Memory usage	8 Gb	1.2 Gb	400 Mb	250 Mb
Compression ratio	1	6.7	20	32
CPU time[a]	74 s	30 s	17 s	24 s
L2 error[a]	0	2.5×10^{-7}	6.2×10^{-5}	1.8×10^{-4}

[a]CPU time measured for the forward Krylov iterative solution to the scalar IE. L2 error measured at the surface of the Earth relative to the forward solution without compression.

further optimization potential of compression error allowance, leading to even more significant efficiency-improving potential of the recursive compression scheme in the forward solutions of vector EM IE induction modelling.

It is perhaps worth mentioning that computation of the recursive SVD compression add a non-trivial cost to the computation of the Green's function matrix. For example, in the vector case, these compressions took on average a little less than half an hour for the $\phi\phi$ component on a single CPU core at 2.2 GHz with 6 Gb memory. However, cost of these compressions is still insignificant compared to the computation of the tensor Green's function

Table 2. Comparison of compression and vector multiplication of the $\phi\phi$ component of the tensor Green's function discretized on the $128 \times 256 \times 16$ numerical grid.

Compression error	0 per cent	0.1 per cent	1 per cent	5 per cent
Memory usage	8 Gb	1.6 Gb	100 Mb	24 Mb
Compression ratio	1	5.2	83	341
CPU time[a]	5.2 s	3.5 s	0.8 s	0.5 s
L2 error[a]	0	0.018	0.023	0.026

[a]CPU time measured for one multiplication on a random vector. L2 error measured in the multiplication result relative to the result without compression: Note that they are significantly larger than those from Table 1. In Table 1, errors are measured in the solutions only at the surface of the Earth, which are extremely insensitive to errors in the larger part of the Green's function matrix accounting for interactions in the deeper interior of the Earth.

components. Furthermore these compressions are easily parallelized, since no communications among the tensor components or the Fourier components are necessary. For EM induction inverse problems, these computations are one-time cost, negligible if compared with the iterative inversions.

6 CONCLUSION

We have developed a simple and effective compression method for the EM Green's function encountered in IE-based modelling of global geomagnetic induction. This method is based on recursively approximating the off-diagonal submatrices of the diagonal-dominant Green's function using SVD-based low-rank approximations. Adoption of this method by a pre-existing IE-based EM modelling code amounts only to a compression procedure of the Green's function matrix. No major modifications are necessary. Numerical examples for a simplified induction model demonstrate significant improvement of computational efficiency of a Krylov subspace forward solver, in terms of both CPU time and memory usage. Application of this compression method in a realistic EM induction model shows great potential in the same direction as in the scalar model. This compression method is expected to be particularly effective in 3-D inversions as well as multiple-source forward simulations of global induction, where Krylov subspace forward solutions have to be performed repeatedly.

ACKNOWLEDGEMENTS

This work has been supported by the European Space Agency through ESTEC contract No. 4000102140/10/NL/JA, and in part by the Russian Foundation for Basic Research under grant No. 13-05-12111. The authors would like to specially thank Dr Koyama for careful and attentive reviews of the manuscript with detailed corrections and valuable advices.

REFERENCES

Avdeev, D., Kuvshinov, A., Pankratov, O. & Newman, G., 2002. Three dimensional induction logging problems, Part I: an integral equation solution and model comparisons, *Geophysics,* **67,** 413–426.

Chew, W.C., Jin, J.M., Lu, C.C., Michielssen, E. & Song, J.M., 1997. Fast solution methods in electromagnetics, *IEEE Trans. Ant. Prop.,* **45,** 533–543.

Fainberg, E.B., Kuvshinov, A.V. & Singer, B.Sh., 1990. Electromagnetic induction in a spherical earth with non-uniform oceans and continents in electric contact with the underlying medium – I. Theory, method and example, *Geophys. J. Int.,* **102,** 273–281.

Hursan, G. & Zhdanov, M., 2002. Contraction integral equation method in three-dimensional electromagnetic modeling, *Radio Sci.,* **37,** doi: 10.1029/2001RS002513.

Koyama, T., 2001. A study on the electrical conductivity of the mantle by voltage measurements of submarine cables, *PhD thesis,* University of Tokyo.

Koyama, T., Khan, A. & Kuvshinov, A., 2014. Three-dimensional electrical conductivity structure beneath Australia from inversion of geomagnetic observatory data: evidence for lateral variations in transition-zone temperature, water content and melt, *Geophys. J. Int.,* **196,** 1330–1350.

Kuvshinov, A., 2008. 3-D Global Induction in the oceans and solid earth: recent progress in modeling magnetic and electric fields from sources of magnetospheric, ionospheric and oceanic origin, *Surv. Geophys.,* **29**(2), 139–186.

Kuvshinov, A. & Semenov, A., 2011. Global 3-D imaging of mantle electrical conductivity based on inversion of observatory C-responses – I. An approach and its verification, *Geophys. J. Int.,* **189,** 1335–1352.

Kuvshinov, A.V., Avdeev, D.B., Pankratov, O.V., Golyshev, S.A. & Olsen, N., 2002. Modelling electromagnetic fields in 3D spherical Earth using fast integral equation approach, in *3D Electromagnetics,* Chap. 3, pp. 43–54, eds Zhdanov, M.S. & Wannamaker, P.E., Elsevier.

Lu, C.C. & Chew, W.C., 1994. A multilevel algorithm for solving boundary-value scattering, *Micro. Opt. Tech. Lett.,* **7,** 466–470.

Michielssen, E. & Boag, A., 1994. Multilevel evaluation of electromagnetic fields for the rapid solution of scattering problems, *Micro. Opt. Tech. Lett.,* **7,** 790–795.

Michielssen, E. & Boag, A., 1996. A multilevel matrix decomposition algorithm for analyzing scattering from large structures, *IEEE Trans. Ant. Prop.,* **44,** 1086–1093.

Pankratov, O., Avdeev, D.B. & Kuvshinov, A., 1995. Electromagnetic field scattering in a homogeneous Earth: a solution to the forward problem, *Phys. Solid. Earth,* **31,** 201–209.

Rokhlin, V., 1990. Rapid solution of integral equations of scattering theory in two dimensions, *J. Comp. Phys.,* **36,** 414–439.

Rius, J.M., Parron, J., Heldring, A., Tamayo, J.M. & Ubeda, E., 2008. Fast iterative solution of integral equations with method of moments and matrix decomposition algorithm—singular value decomposition, *IEEE Trans. Ant. Prop.,* **56,** 2314–2324.

Singer, B.S., 1995. Method for solution of Maxwell's equations in non-uniform media, *Geophys. J. Int.,* **120**(3), 590–598.

Singer, B.Sh., 2008. Electromagnetic integral equation approach based on contraction operator and solution optimization in Krylov subspace, *Geophys. J. Int.,* **175,** 857–884.

Sun, J. & Egbert, G., 2012a. A thin-sheet model for global electromagnetic induction, *Geophys. J. Int.,* **189,** 343–356.

Sun, J. & Egbert, G., 2012b. Spherical decomposition of electromagnetic fields generated by quasi-static currents, *Int. J. Geomath.,* **3,** 279–295.

APPENDIX A: DERIVATION OF THE SCALAR CONTRACTION OPERATOR

Consider the scalar wave equation without conductivity perturbation and with an arbitrary source S,

$$\nabla^2\Phi + k_b^2\Phi = -\mathrm{i}\omega\mu_0 S\,, \tag{A1}$$

with the solution given by

$$\Phi(\mathbf{r}) = \int \mathrm{d}^3 r' g(\mathbf{r}, \mathbf{r}') S(\mathbf{r}')\,. \tag{A2}$$

Multiplying both sides of (A1) by Φ^*, where * refers to complex conjugate, and integrating over the entire space, we obtain

$$\int \mathrm{d}^3 r \left[-|\nabla\Phi|^2 + \mathrm{i}\omega\mu_0\sigma_b|\Phi|^2 + \mathrm{i}\omega\mu_0 S\Phi^*\right] = 0\,, \tag{A3}$$

where $k_b^2 = \mathrm{i}\omega\mu_0\sigma_b$, and integration by parts and appropriate boundary condition at infinity has been invoked. Taking the imaginary part of (A3), we further obtain

$$\int \mathrm{d}^3 r\, [\sigma_b |\Phi|^2 + \Re\{S\Phi^*\}] = 0\,. \tag{A4}$$

If S is supported on a finite (secondary) source domain Ω, (A4) becomes

$$\int \mathrm{d}^3 r\, \sigma_b |\Phi|^2 + \int_\Omega \mathrm{d}^3 r\, \Re\{S\Phi^*\} = 0\,, \tag{A5}$$

which implies

$$\int_\Omega \mathrm{d}^3 r\, \sigma_b |\Phi|^2 + \int_\Omega \mathrm{d}^3 r\, \Re\{S\Phi^*\} \le 0\,, \tag{A6}$$

or equivalently

$$\int_\Omega \mathrm{d}^3 r\, |2\sigma_b \Phi + S|^2 \le \int_\Omega \mathrm{d}^3 r\, |S|^2\,. \tag{A7}$$

Considering (A2), it is seen that (A7) implies

$$\|2\sigma_b g(S) + S\| := \|\gamma(S)\| \le \|S\|\,, \tag{A8}$$

where $\|\Phi\|^2 = \int_\Omega \mathrm{d}^3 r\, |\Phi|^2$ denotes the L_2 norm of an arbitrary scalar field Φ over the source domain Ω. Evidently the transformed operator $\gamma = 2\sigma_b g + \delta$ has operator norm $\|\gamma\| \le 1$, and (9) is convergent.

APPENDIX B: GREEN'S FUNCTION FOR A TWO-LAYER SPHERE

The scalar GF as defined in (8) is needed in the implementation of the iterative solution. For simplicity, we consider the case of a two-layer Earth of outer radius r_0 with an infinitely conductive core of inner radius r_1 situated in the free space. The conductivity of the outer layer is σ_1. The Earth is covered by a conductive thin crust of conductance τ_1. In other words,

$$k_b(r) = \begin{cases} k_0, & r > r_0 \\ k_1, & r_1 < r < r_0 \end{cases}\,, \tag{B1}$$

where $k_0 = \omega\sqrt{\mu_0\epsilon_0}$ is the free-space wavenumber, and $k_1 = \sqrt{\mathrm{i}\omega\mu_0\sigma_1}$ is the complex wave number of the Earth's interior. The GF $g(\mathbf{r}, \mathbf{r}')$ with the source point $\mathbf{r}'$ located inside the Earth consists of two parts for its interior response, that is a direct field $g_1(\mathbf{r}, \mathbf{r}')$ and an internal and a external reflected field $g_r(\mathbf{r}, \mathbf{r}')$. The exterior response is the transmitted field $g_t(\mathbf{r}, \mathbf{r}')$. The direct field is an out-going spherical wave given by

$$g_1(\mathbf{r}, \mathbf{r}') = \mathrm{i}\omega\mu_0 \frac{\mathrm{e}^{\mathrm{i}k_1|\mathbf{r}-\mathbf{r}'|}}{4\pi|\mathbf{r}-\mathbf{r}'|}\,, \tag{B2}$$

which assumes a centred spherical wave decomposition

$$g_1(\mathbf{r}, \mathbf{r}') = -\omega\mu_0 k_1 \sum_{l=0}^{\infty} j_l(k_1 r_i) h_l(k_1 r_e) \sum_{m=-l}^{l} Y_l^m(\theta, \phi) Y_l^{m*}(\theta', \phi'), \tag{B3}$$

where $r_i = \min(r, r')$, $r_e = \max(r, r')$, $j_l(\,\cdot\,)$ and $h_l(\,\cdot\,)$ are lth degree Bessel functions of the first and third kind, and $Y_l^m(\cdot)$ is the spherical harmonic of degree l and order m. The reflected and transmitted fields are given by

$$g_r(\mathbf{r}, \mathbf{r}') = -\omega\mu_0 k_1 \sum_{l=0}^{\infty} [C_l j_l(k_1 r) + D_l h_l(k_1 r)] \times \sum_{m=-l}^{l} Y_l^m(\theta, \phi) Y_l^{m*}(\theta', \phi')\,, \tag{B4}$$

where C_l and D_l coefficients of degree l represent reflected fields of external and internal origins, respectively, and

$$g_t(\mathbf{r}, \mathbf{r}') = -\omega\mu_0 k_1 \sum_{l=0}^{\infty} T_l \left(\frac{r_0}{r}\right)^{l+1} \sum_{m=-l}^{l} Y_l^m(\theta, \phi) Y_l^{m*}(\theta', \phi')\,, \tag{B5}$$

where T_l coefficient of degree l represents transmitted field outside the Earth. The GF $g(\mathbf{r}, \mathbf{r}')$ is given by

$$g(\mathbf{r}, \mathbf{r}') = \begin{cases} g_t(\mathbf{r}, \mathbf{r}') & r > r_0 \\ g_1(\mathbf{r}, \mathbf{r}') + g_r(\mathbf{r}, \mathbf{r}') & r_1 < r < r_0 \end{cases}\,, \tag{B6}$$

and $g(\mathbf{r}, \mathbf{r}') \equiv 0$ inside the core. The coefficients C_l, D_l and T_l can be obtained by enforcing boundary condition at the interface,

$$\begin{aligned} &g(\mathbf{r}, \mathbf{r}')|_{r=r_{0-}}^{r=r_{0+}} = 0, \\ &\partial_r g(\mathbf{r}, \mathbf{r}')|_{r=r_{0-}}^{r=r_{0+}} + i\omega\mu_0\tau_1 g(\mathbf{r}, \mathbf{r}')|_{r=r_0} = 0, \\ &g(\mathbf{r}, \mathbf{r}')|_{r=r_{1+}} = 0\,. \end{aligned} \tag{B7}$$

The unknown coefficients in (B2), (B4), (B5) and (B6) may be obtained by enforcing the boundary conditions (B7) componentwise and solving the resulting systems of equations numerically.